The Snuffle Problem

Denev

for the Numerical Simulation of a Microreactor

July 2007

The following problem definition is a copy of the Internal Report "A test case for microreactor flows - a two-dimensional jet in crossflow with chemical reaction" by Carlos J. Falconi, Jordan A. Denev, Jochen Fröhlich and Henning Bockhorn that is available at `http://www.ict.uni-karlsruhe.de/index.pl/themen/dns/index.html`: "2d test case for microreactor flows. Internal report. 2007".

A test case for microreactor flows - a two-dimensional jet in crossflow with chemical reaction
- Internal Report -

Carlos J. Falconi, Jordan A. Denev, Jochen Fröhlich, Henning Bockhorn
Institute for Technical Chemistry und Polymer Chemistry
University of Karlsruhe (TH)
Kaiserstraße 12, 76128 Karlsruhe, Germany
www.ict.uni-karlsruhe.de

December 15, 2006; revised: July 20, 2007

1 Introduction

This report presents a test configuration suitable for the validation of numerical methods to treat mixing and chemical reactions. It is inspired by the jet in cross flow situation depicted in Fig. 1. A laminar jet exits from a pipe duct, perpendicular to the main flow in a channel. The inflow conditions for the jet and the cross flow are given by two different prescribed velocity profiles. Two reactive scalars, introduced in the jet and the cross flow, respectively, are used to investigate the reaction rate, as it would occur in a diffusion flame. The reactive scalars are passive with respect to the velocity field. Here, the two-dimensional equivalent of the situation in Fig. 1 is considered. Simulations were performed with a velocity ratio between jet and cross flow of 1.5 at a Reynolds number of 25. A three-dimensional code was employed, using a single cell in spannwise direction. The computed reference solution is steady.

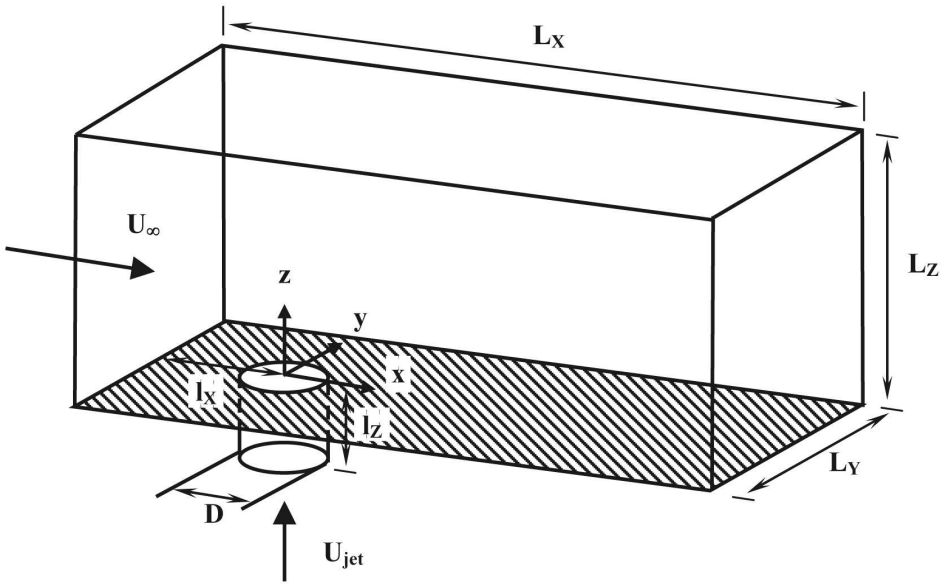

Figure 1: Configuration of the simulation

2 Geometry and parameters

The origin of the coordinate system is in the middle of the pipe, at the exit of the jet (Fig. 1), with x being the streamwise, y the spannwise and z the wall normal coordinate, respectively.

The geometry is the two-dimensional equivalent of the one depicted in Fig. 1. It is defined by the parameters

$D = 1$; $L_x = 16$; $L_y = 0.1^*$; $L_z = 4$; $l_x = 3.5$; $l_z = 2$

*(cf. Introduction)

3 Basic equations

For generality, the equations are provided in their three-dimensional version here. Spacial coordinates are x in streamwise, y in spanwise, and z in wall-normal direction, with velocity components (u, v, w); p is pressure, ρ density, μ dynamic viscosity, and $\nu = \mu/\rho$ the kinematic viscosity. Nondimensional equations are used with reference length being the diameter D of the jet and reference velocity the velocity U_∞ of the cross flow. Density is assumed constant (i.e. equal in jet and crossflow), buonyancy hence does not occur. Mass fractions are denoted by Y, reaction rates by ω, and diffusion coefficients by Γ. The equations then read

- Continuity equation:

$$\frac{\partial u}{\partial x} + \frac{\partial v}{\partial y} + \frac{\partial w}{\partial z} = 0 \tag{1}$$

- Momentum equations:

$$\rho\,(\frac{\partial u}{\partial t} + u\frac{\partial u}{\partial x} + v\frac{\partial u}{\partial y} + w\frac{\partial u}{\partial z}) = -\frac{\partial p}{\partial x} + \mu\,(\frac{\partial^2 u}{\partial x^2} + \frac{\partial^2 u}{\partial y^2} + \frac{\partial^2 u}{\partial z^2}) \tag{2}$$

$$\rho\,(\frac{\partial v}{\partial t} + u\frac{\partial v}{\partial x} + v\frac{\partial v}{\partial y} + w\frac{\partial v}{\partial z}) = -\frac{\partial p}{\partial y} + \mu\,(\frac{\partial^2 v}{\partial x^2} + \frac{\partial^2 v}{\partial y^2} + \frac{\partial^2 v}{\partial z^2}) \tag{3}$$

$$\rho\,(\frac{\partial w}{\partial t} + u\frac{\partial w}{\partial x} + v\frac{\partial w}{\partial y} + w\frac{\partial w}{\partial z}) = -\frac{\partial p}{\partial z} + \mu\,(\frac{\partial^2 w}{\partial x^2} + \frac{\partial^2 w}{\partial y^2} + \frac{\partial^2 w}{\partial z^2}) \tag{4}$$

- Chemistry

  Two reactive scalars are introduces, scalar A with the jet, scalar B with the cross flow reacting to the product Q.

$$A + B \xrightarrow{Da} Q \tag{5}$$

- Transport of scalar quantities

$$\rho\,(\frac{\partial Y_A}{\partial t} + u\frac{\partial Y_A}{\partial x} + v\frac{\partial Y_A}{\partial y} + w\frac{\partial Y_A}{\partial z}) = \rho\,\Gamma_A\,(\frac{\partial^2 Y_A}{\partial x^2} + \frac{\partial^2 Y_A}{\partial y^2} + \frac{\partial^2 Y_A}{\partial z^2}) + \omega_A \tag{6}$$

$$\omega_A = -Da\ Y_A\ Y_B$$

$$\rho\,(\frac{\partial Y_B}{\partial t} + u\frac{\partial Y_B}{\partial x} + v\frac{\partial Y_B}{\partial y} + w\frac{\partial Y_B}{\partial z}) = \rho\,\Gamma_B\,(\frac{\partial^2 Y_B}{\partial x^2} + \frac{\partial^2 Y_B}{\partial y^2} + \frac{\partial^2 Y_B}{\partial z^2}) + \omega_B \tag{7}$$

$$\omega_B = \omega_A$$

- Reaction product Q:

$$Y_Q = 1 - Y_A - Y_B \tag{8}$$

4 Characteristic numbers

- Velocities and Reynolds number:

  Reference velocity is the crossflow velocity far from the wall U_∞. The jet velocity U_{jet} is the mean velocity in the pipe. The ratio of both is $R = \frac{U_{jet}}{U_\infty}$. The Reynolds number is defined as $Re_\infty = \frac{U_\infty D}{\nu}$. The present case is defined with $R = 1.5$ and $Re = 25$.

- Scalar properties:

  The following physical properties are chosen $\rho = const.$, $\Gamma_A = \Gamma_B = \Gamma_Q = \Gamma$, $Sc = 1$, $Da = 1$.

- Dimensionless form of equations

  If the above notation of the transport equations is used the natural choice of reference quantities leads to posing $\rho = 1$, $\nu = 1/Re$, $\Gamma = 1/Re$.

5 Boundary conditions

Using the above reference quantities the following boundary conditions are specified in non-dimensional form.

- Cross flow: entry of the main channel

$$\begin{aligned} u &= 1 - e^{-5\zeta} \qquad , \qquad \zeta = min\ (\ z, L_z - z\ ) \\ w &= 0 \\ Y_A &= 0 \\ Y_B &= 1 \\ Y_Q &= 0 \end{aligned} \tag{9}$$

- Entry of pipe

$$\begin{aligned} u &= 0 \\ w &= R\ 2\ (\ 1 - (2r)^2\ ), \qquad r = x \\ Y_A &= 1 \\ Y_B &= 0 \\ Y_Q &= 0 \end{aligned}$$

- Exit of main channel: Homogeneous Neumann condition, i.e. gradient equal to zero for all quantities.

- Top and and bottom wall: no slip for the velocities and vanishing wall-normal gradient for the scalars.

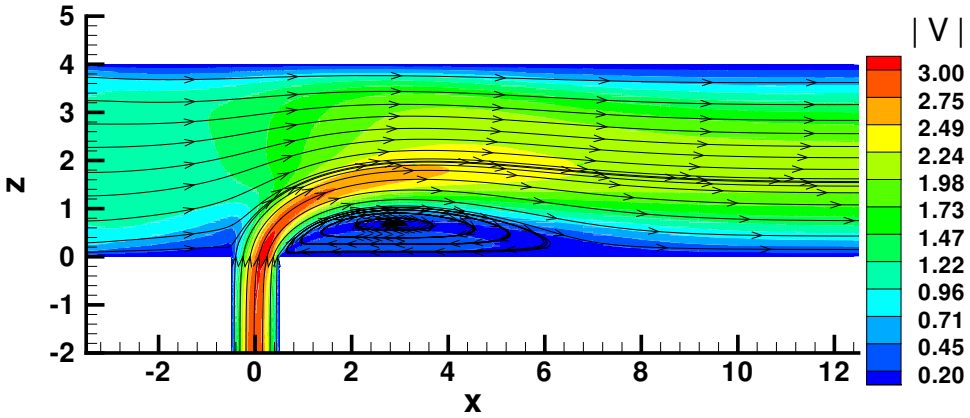

Figure 2: Streamlines and velocity magnitude $|V|$.

6 Results:

A reference computation was done, employing the code LESOCC2 previously used for the turbulent three-dimensional configuration [1]. It solves the three-dimensional incompressible unsteady Navier-Stokes equations using a central second-order finite volume discrization for all derivatives in space and multi-block structure grid treatment for complex geometry. The time scheme is a second order three-stage Runge-Kutta scheme.

The domain is discretized with 20800 cells. In the pipe 55 cells in x-direction have been used with uniform spacing, while in z-direction the grid is clustered near the outlet of the pipe, using 44 cells with

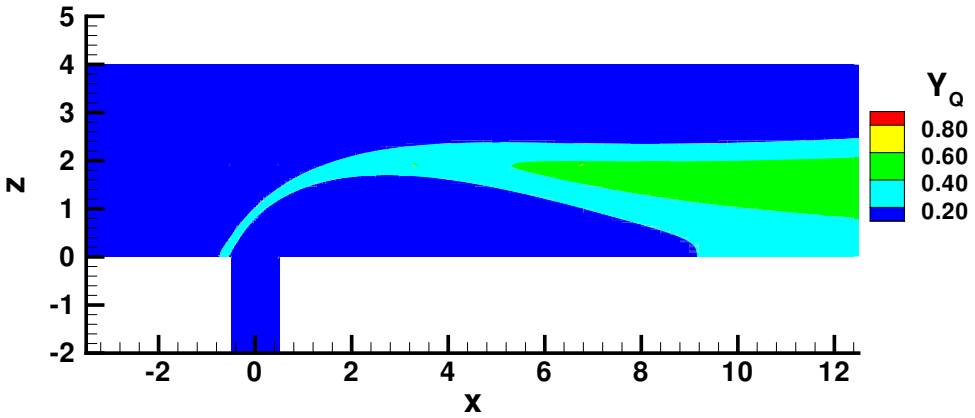

Figure 3: Countour plot of the mass fraction of the product Y_Q.

a stretching of 1.03. In the channel the grid in x-direction is clustered near the pipe outlet with 44 cells before the pipe outlet and 92 cells after the pipe outlet, using a stretching of 1.04. In z-direction, the grid in the main channel is clustered near the top and bottom walls using 100 cells with a stretching of 1.03. The minimal cell size in x-, and z-direction ($\triangle x_{min}$, $\triangle z_{min}$) are equal to 0.02 D, while the maximun cell size in x-, and z-direction ($\triangle x_{max}$, $\triangle z_{max}$) are equal to 0.2 D and 0.07 D, respectively. In $y-$direction, single cell was used as stated above.

A laminar steady state solution was obtained. Streamlines are visualized in Fig. 2. They show that for these values of the paramters a closed recirculation bubble is obtained downstream of the outlet. The velocity magnitude is also presented in the figure. Fig. 3 presents the mass fraction of the product Y_Q.

Detailed results for all quantities are available in Tecplot format and can be downloaded from: *http://www.ict.uni-karlsruhe.de/index.pl/themen/dns/index.html*. (2d test case for microreactor flows - internal report, 2007 + 2djicfreaction.dat).

References

[1] J. Fröhlich, J.A. Denev, and H. Bockhorn. Large eddy simulation of a jet in crossflow. In *Proceedings of ECCOMAS 2004, Jyväskylä, Finland, July 24-28, ISBN 951-39-1868-8, CD-ROM*, Barcelona, 2004. CIMNE.

Results of the Snuffle Problem Denev by the FDEM Program

Torsten Adolph and Willi Schönauer

Forschungszentrum Karlsruhe, Institute for Scientific Computing,
Hermann-von-Helmholtz-Platz 1, 76344 Eggenstein-Leopoldshafen, Germany
{torsten.adolph,willi.schoenauer}@iwr.fzk.de
http://www.fzk.de/iwr

1 Introduction

This paper describes a further "snuffle problem" for the application of the FDEM (Finite Difference Element Method). The FDEM [2] has been developed with the support of the German Ministry of Research. The ministry has obliged us to demonstrate the usefulness of FDEM in cooperations with Industry and Research. Before we enter a cooperation, we solve a snuffle problem that the partner can see what we can do and we can see what he wants.

The unique feature of FDEM is its property to compute together with the solution an error estimate so that we know the quality of the solution. The standard software packages that are used by the engineers do not deliver error estimates for the discretization errors. Therefore, users try to get information about the quality of the solution by mesh refinement tests, but this is a doubtful and cumbersome procedure. When such users make error investigations, they ask: How good is my solution. For FDEM we ask: How good is my error estimate. This is one level higher quality. Up to now engineering problems like the present one have never been solved with the inclusion of an error estimate. So we solve these problems for the first time with the inclusion of an error estimate. This shows clearly the numerical difficulties and points to the mathematical singularities of the problem. We can see in the present problem where large errors occur at salient corners. Here the Navier-Stokes equations have a singularity.

2 The numerical solution

We simulate numerically the mixing and the chemical reactions in a microreactor. Here a laminar jet enters from a pipe, perpendicular to the main flow in a channel. The inflow conditions for the jet and the cross flow are given by two different prescribed velocity profiles. Chemical component B enters in the main channel, by the side channel component A is entered. Fig. 1 shows the configuration of the investigated microreactor. We assume an incompressible fluid with Reynolds number 25 where the chemical components A and B are reacting and produce component Q.

The mass fractions of A, B, Q are denoted by Y_A, Y_B, Y_Q. We use the following notations: velocity components u, w, pressure p, density ρ, dynamical viscosity μ, diffusion coefficient Γ.

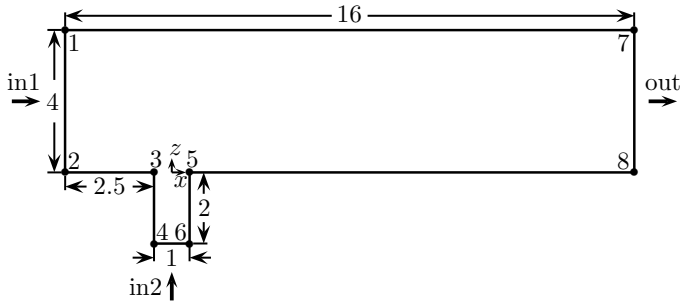

Fig. 1. Configuration of the investigated microreactor in 2-D.

As prescribed in the problem definition [1], we use nondimensional equations with reference length being the diameter D of the jet and reference velocity the velocity U_∞ of the cross flow. The PDEs given in the problem definition [1] are simplified for the 2-D situation, so it holds the following system of six PDEs for the six variables u, w, p, Y_A, Y_B, Y_Q:

- continuity equation for the mixture

$$\frac{\partial u}{\partial x} + \frac{\partial w}{\partial z} = 0, \tag{1}$$

- two momentum equations for the mixture

$$\rho\left(u\frac{\partial u}{\partial x} + w\frac{\partial u}{\partial z}\right) = -\frac{\partial p}{\partial x} + \mu\left(\frac{\partial^2 u}{\partial x^2} + \frac{\partial^2 u}{\partial z^2}\right), \tag{2}$$

$$\rho\left(u\frac{\partial w}{\partial x} + w\frac{\partial w}{\partial z}\right) = -\frac{\partial p}{\partial z} + \mu\left(\frac{\partial^2 w}{\partial x^2} + \frac{\partial^2 w}{\partial z^2}\right), \tag{3}$$

- two continuity equations for the components Y_A, Y_B

$$\rho\left(u\frac{\partial Y_A}{\partial x} + w\frac{\partial Y_A}{\partial z}\right) = \rho\Gamma_A\left(\frac{\partial^2 Y_A}{\partial x^2} + \frac{\partial^2 Y_A}{\partial z^2}\right) - D_a Y_A Y_B, \tag{4}$$

$$\rho\left(u\frac{\partial Y_B}{\partial x} + w\frac{\partial Y_B}{\partial z}\right) = \rho\Gamma_B\left(\frac{\partial^2 Y_B}{\partial x^2} + \frac{\partial^2 Y_B}{\partial z^2}\right) - D_a Y_A Y_B, \tag{5}$$

- Dalton's law

$$Y_Q = 1 - Y_A - Y_B. \tag{6}$$

In Table 1 we show which equation is used in which position in the system of PDEs for the nodes in the interior of the domain.

The next problem we want to discuss are the boundary conditions for the six types of boundaries ① to ⑥ of Fig. 2. In the right corners, we need some BCs from the upper/lower boundary ④ and some BCs of the right boundary ③, so these corner nodes have to be defined as an additional boundary.

Table 1. Sequence of variables and equations in the interior of the domain.

No.	Var.	equation
1	u	(1)
2	w	(3)
3	p	(2)
4	Y_A	(4)
5	Y_B	(5)
6	Y_Q	(6)

Fig. 2. Numbering of the external boundaries of the solution domain.

At the boundaries, for some variables BCs are given. However, we need at each boundary six equations for six variables. So we take the missing equations quite naturally from the set of interior equations, where no other conditions, e.g. symmetry at boundary ③, are given. The BCs for the six external boundaries are given in Table 2.

Table 2. Sequence of variables and equations at the boundaries ①–⑥ of the domain.

Var.	①	②	③	④	⑤	⑥
u	see [1, Sect.5]	$u = 0$	$\frac{\partial u}{\partial x} = 0$	$u = 0$	$u = 0$	$u = 0$
w	$w = 0$	see [1, Sect.5]	$\frac{\partial w}{\partial x} = 0$	$w = 0$	$w = 0$	$w = 0$
p	eq. (2)	$p = p_{atm}$	eq. (2)	eq. (3)	eq. (3)	eq. (2)
Y_A	$Y_A = 0$	$Y_A = 1$	$\frac{\partial Y_A}{\partial x} = 0$	$\frac{\partial Y_A}{\partial y} = 0$	$\frac{\partial Y_A}{\partial x} = 0$	$\frac{\partial Y_A}{\partial y} = 0$
Y_B	$Y_B = 1$	$Y_B = 0$	$\frac{\partial Y_B}{\partial x} = 0$	$\frac{\partial Y_B}{\partial y} = 0$	$\frac{\partial Y_B}{\partial x} = 0$	$\frac{\partial Y_B}{\partial y} = 0$
Y_Q	$Y_Q = 0$	$Y_Q = 0$	$\frac{\partial Y_Q}{\partial x} = 0$	$\frac{\partial Y_Q}{\partial y} = 0$	$\frac{\partial Y_Q}{\partial x} = 0$	$\frac{\partial Y_Q}{\partial y} = 0$

We use the following values for the material data:

$$\rho = 1, \quad \mu = 0.04, \quad \Gamma_A = \Gamma_B = 0.04, \quad D_a = 1. \tag{7}$$

We use three different grids for the computations. We start with a grid with 641×161 nodes in the main channel and 41×81 nodes in the pipe which yields 106,481 nodes. The second grid results from a complete mesh refinement of the first grid, and by another complete mesh refinement, we get the third grid with 2561×641 nodes in the main channel and 161×321 nodes in the pipe which yields 1,693,121 nodes and 10,158,726 unknowns, see Table 3.

Table 3. Grids for the simulation of a microreactor.

Grid	Dimensions		Number of		
no.	main channel	pipe	nodes	elements	unknowns
1	641×161	41×81	106,481	211,200	638,886
2	1281×321	81×161	424,161	844,800	2,544,966
3	2561×641	161×321	1,693,121	3,379,200	10,158,726

We compute with consistency order $q = 4$, and we use 128 processors. The computations are carried out on two supercomputers: The first one is the HP XC4000 with 2.6 GHz AMD Opteron processors and InfiniBand 4X interconnect that has been installed at the University of Karlsruhe, Germany. The second supercomputer is the SGI Altix 4700 with 1.6 GHz Intel Itanium2 Montecito Dual Core processors and NUMAlink 4 interconnect at the LRZ Munich, Germany.

We first solved only the system of PDEs with the three variables u, w, p for the flow through the microreactor. The number of unknowns is half the number of unknowns given in Table 3 here. The results of these computations for the three grids are presented in Table 4.

Table 4. Results of the flow through a microreactor.

Grid		max.	global relat. estim. error		CPU time [sec]	
no.	Var.	solution	max.	mean	HP XC4000	SGI Altix 4700
1	u	2.434	10.1	$0.11 \cdot 10^{0}$	348.97	526.61
	w	3.000	18.8	$0.45 \cdot 10^{-1}$		
	p	$0.100 \cdot 10^{6}$	$0.61 \cdot 10^{-2}$	$0.43 \cdot 10^{-3}$		
2	u	2.518	8.73	$0.47 \cdot 10^{-1}$	2169.51	2961.00
	w	3.000	15.0	$0.19 \cdot 10^{-1}$		
	p	$0.100 \cdot 10^{6}$	$0.13 \cdot 10^{-1}$	$0.99 \cdot 10^{-3}$		
3	u	2.660	3.10	$0.12 \cdot 10^{-1}$	35169.05	43164.07
	w	3.013	1.96	$0.46 \cdot 10^{-2}$		
	p	$0.100 \cdot 10^{6}$	$0.42 \cdot 10^{-2}$	$0.23 \cdot 10^{-2}$		

We want to discuss the arithmetic performance of the two computers by the timings given in Table 4. The HP has AMD Opteron processors of 2.6 GHz, so the theoretical peak performance for 64-bit arithmetic for multiply-and-add operations (superscalar speed) is 5.2 GFLOPS/processor. The SGI has Intel Itanium2 Montecito dual core processors of 1.6 GHz, so the theoretical peak performance is $2 \cdot 3.2 = 6.4$ GFLOPS/processor. So we expect that the SGI is faster by a factor $6.4/5.2 = 1.23$. However, from the timings of grid 3 in Table 4, we see that the HP is faster by a factor $43164.07/35169.05 = 1.23$. In [3] it is discussed and shown by measurements for many processors that ultimately, the cache bandwidth and memory bandwidth is decisive for the real arithmetic performance. The CPUs are idling a bigger part of the time, waiting for data. So the HP has obviously a better relative bandwidth than the SGI because the relative bandwidth for the dual core Itanium2 is worse.

Afterwards, we computed the system of PDEs with the variables Y_A, Y_B, Y_Q for the chemical reaction in the microreactor. Again, the number of unknowns is half the number of unknowns given in Table 3. For each of the three computations, we read in the solution for

Table 5. Results of the chemical reaction in a microreactor.

Grid no.	Var.	max. solution	global relat. estim. error max.	global relat. estim. error mean	CPU time [sec] HP XC 4000	CPU time [sec] SGI Altix 4700
1	Y_A	1.444	4.27	$0.68 \cdot 10^{-2}$	145.13	219.70
	Y_B	1.000	4.07	$0.70 \cdot 10^{-2}$		
	Y_Q	0.609	3.93	$0.12 \cdot 10^{-1}$		
2	Y_A	1.061	2.13	$0.14 \cdot 10^{-2}$	1267.80	1708.29
	Y_B	1.000	1.39	$0.71 \cdot 10^{-3}$		
	Y_Q	0.602	1.45	$0.19 \cdot 10^{-2}$		
3	Y_A	1.000	1.15	$0.14 \cdot 10^{-2}$	16178.16	20362.58
	Y_B	1.000	0.71	$0.85 \cdot 10^{-3}$		
	Y_Q	0.597	0.75	$0.19 \cdot 10^{-2}$		

u, w that we have just computed from the u, w, p-system. This means that the flow velocities u and w are constant for the computation of the chemical components. The results of these computations for the three grids are presented in Table 5.

Table 6. Results of the simulation of a microreactor.

Grid no.	Var.	max. solution	global relat. estim. error max.	global relat. estim. error mean	CPU time [sec] HP XC4000	CPU time [sec] SGI Altix 4700
1	u	2.434	10.1	$0.11 \cdot 10^{0}$	189.10	264.03
	w	3.000	18.8	$0.45 \cdot 10^{-1}$		
	p	$0.100 \cdot 10^{6}$	$0.61 \cdot 10^{-2}$	$0.43 \cdot 10^{-3}$		
	Y_A	1.444	5.96	$0.61 \cdot 10^{-1}$		
	Y_B	1.000	5.93	$0.97 \cdot 10^{-1}$		
	Y_Q	0.609	4.37	$0.12 \cdot 10^{0}$		
2	u	2.518	8.73	$0.47 \cdot 10^{-1}$	2378.02	2612.45
	w	3.000	15.0	$0.19 \cdot 10^{-1}$		
	p	$0.100 \cdot 10^{6}$	$0.13 \cdot 10^{-1}$	$0.99 \cdot 10^{-3}$		
	Y_A	1.061	2.25	$0.27 \cdot 10^{-1}$		
	Y_B	1.000	1.46	$0.37 \cdot 10^{-1}$		
	Y_Q	0.602	1.54	$0.42 \cdot 10^{-1}$		
3	u	2.660	3.10	$0.12 \cdot 10^{-1}$	40450.32	49718.47
	w	3.013	1.96	$0.46 \cdot 10^{-2}$		
	p	$0.100 \cdot 10^{6}$	$0.42 \cdot 10^{-2}$	$0.23 \cdot 10^{-2}$		
	Y_A	1.000	1.23	$0.12 \cdot 10^{-1}$		
	Y_B	1.000	0.78	$0.94 \cdot 10^{-2}$		
	Y_Q	0.597	0.74	$0.24 \cdot 10^{-1}$		

As the system of PDEs for the flow through the microreactor is completely independent (decoupled) from the system of PDEs for the chemical components, it is of no importance for the solution and for the errors of the velocity components and the pressure whether we compute the solution of the two systems with three PDEs each, or the solution of the complete system with six PDEs. However, the velocity field affects the chemical components

so that we get in fact the same solution if we compute the solution of the system with six PDEs but the errors change as there enter the errors of the velocity components.

Thus, the last step is to compute the solution of the system with six PDEs. Here, we read in the solution of the two systems of PDEs with three PDEs that we just computed. Then the computations are finished after one Newton step because the starting solution already is quite good. The results of these computations for the three grids are presented in Table 6.

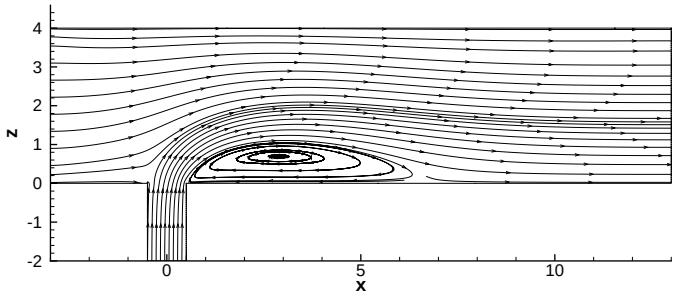

Fig. 3. Plot of the streamlines for the flow through the microreactor.

Figure 3 shows the plot of the streamlines for the flow through the microreactor. In Figs. 4–9, the result corresponding to grid 3 of Table 6 for each variable is plotted as coloured contour plot together with its error.

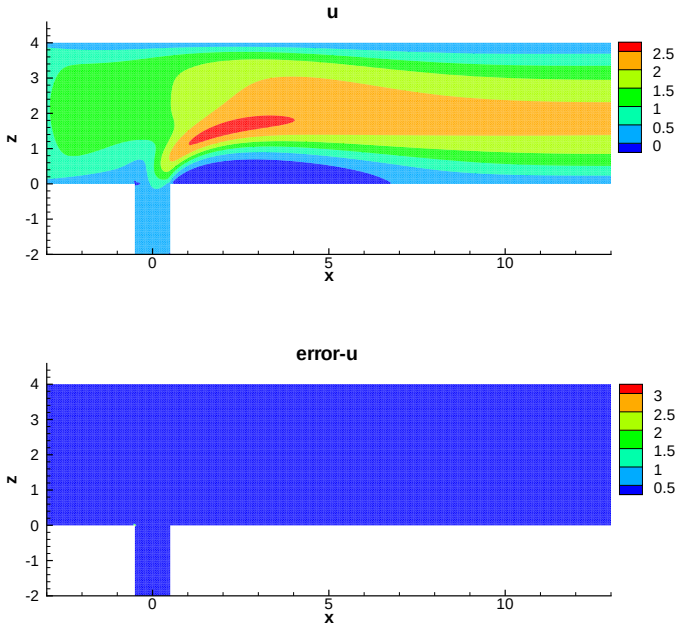

Fig. 4. Contour plot of velocity u and its error.

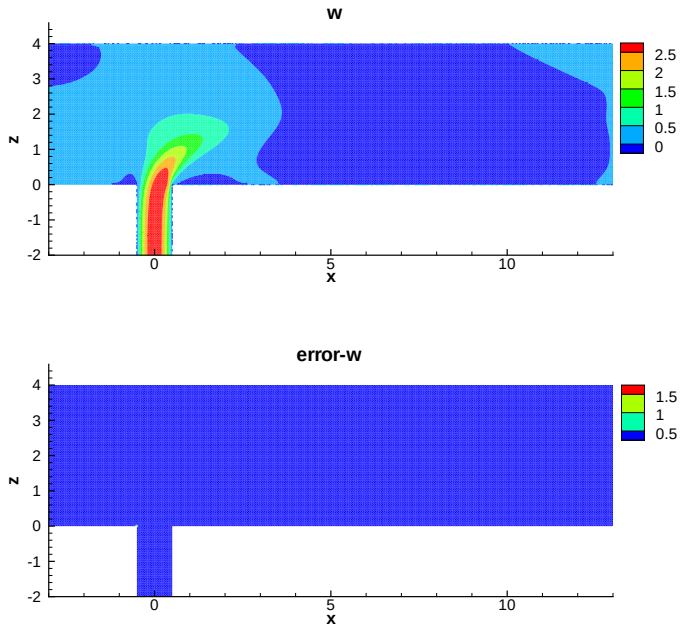

Fig. 5. Contour plot of velocity w and its error.

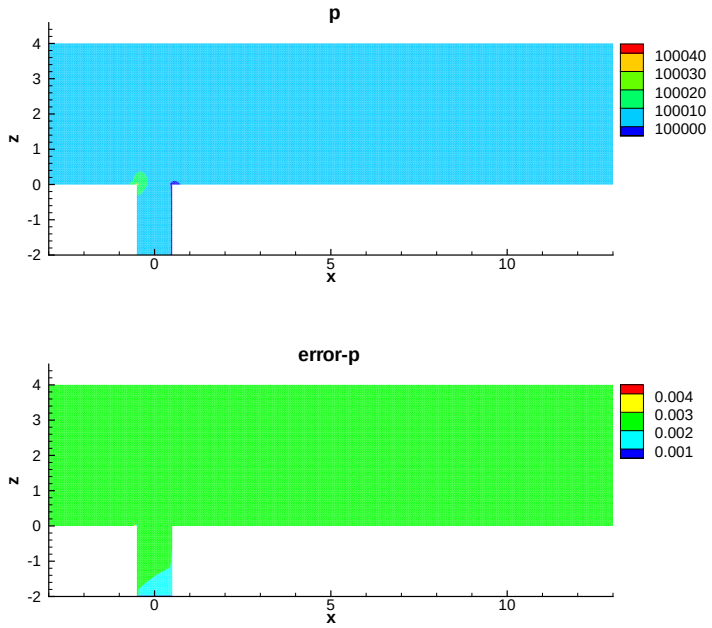

Fig. 6. Contour plot of pressure p and its error.

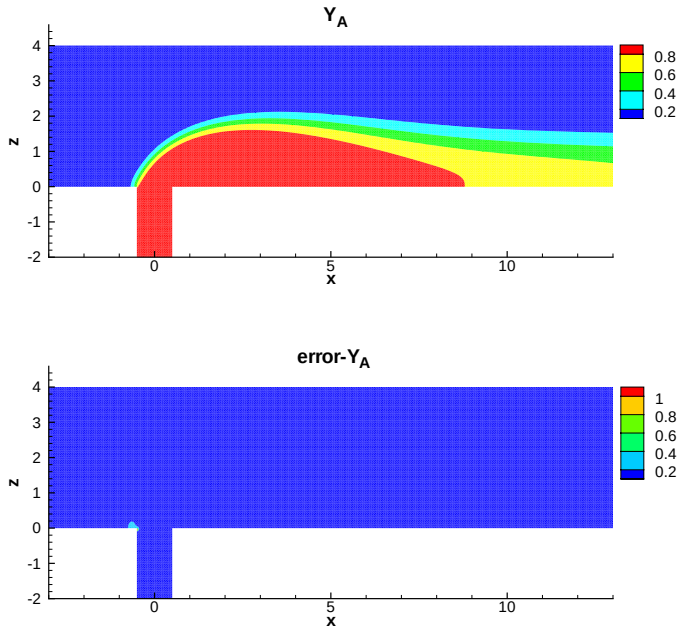

Fig. 7. Contour plot of mass fraction Y_A and its error.

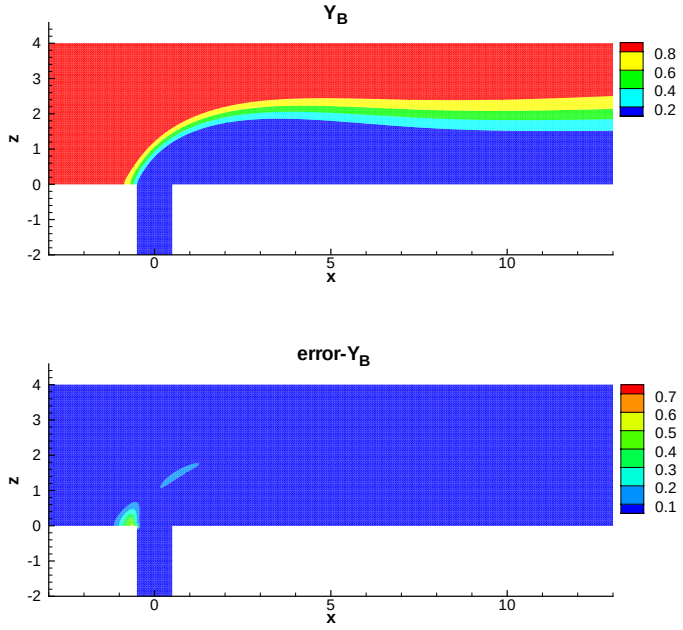

Fig. 8. Contour plot of mass fraction Y_B and its error.

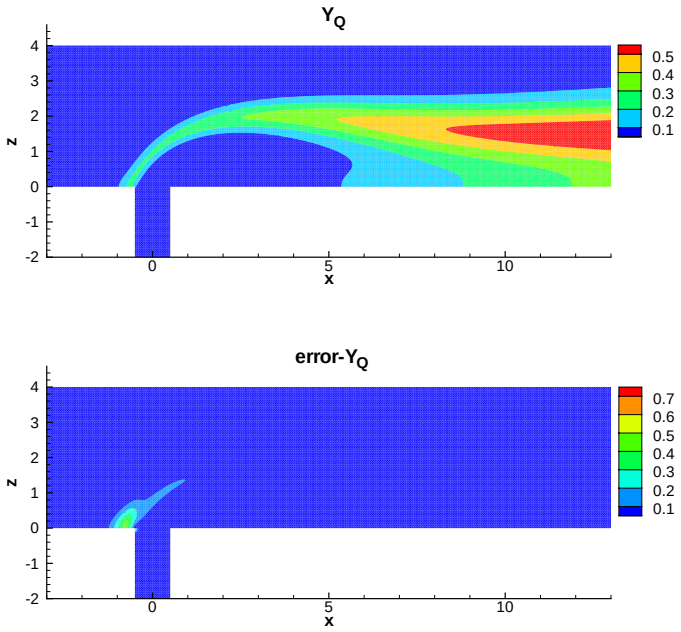

Fig. 9. Contour plot of mass fraction Y_Q and its error.

3 Discussion of the errors and concluding remarks

If we look at the errors in Table 6, we see that the maximum global relative errors are quite large. A maximum error of 3.10 for u for grid 3 means 310%. This is an error that occurs only locally as a consequence of the corner singularity of the Navier-Stokes equations. From the theory of FDEM we know that we obtain a good and reliable error estimate only if the estimated error is small. If it is large, the higher order formula that estimates the error is quite different from the actual order. This is a built-in natural self-control of the error estimate. If we thus get a large error estimate, this tells us only that the error is large, but we then can no longer say how large it is. The mean global relative error for u for grid 3 of $0.12 \cdot 10^{-1}$ means 1.2%. Thus, the arithmetic mean of all errors is in the 1% range and this is the value that is relevant for the engineer. We use a FDM, i.e. here a polynomial approach of the order 4 (would be exact if the solution was a polynomial of 4^{th} order). Such a polynomial cannot approximate well the corner singularity of the Navier-Stokes equations. The underlying physics quite naturally has no singularity, but this occurs at a quite different scale, namely at the molecular level and there is no no-slip condition that causes the singularity. In Figs. 10 and 11, we see blow-ups of the error of u and of Y_Q for the solution of grid 3 in the region where the large errors occur. There is also visible the grid. We see that the large errors occur only locally.

Grid 2 in Table 6 results from a total mesh refinement of grid 1. Refinement is made by halving the edges of each triangle which results in four new triangles. A characteristic length h then becomes $h/2$. As we use a 4^{th} order method, the error should theoretically be reduced by a factor $((h/2)/h)^4 = (1/2)^4 = 1/16 = 0.0625$ or roughly by one order of magnitude. The same holds for the refinement of grid 2 which yields grid 3, see Table 3. So we expect in Table 6 that the errors go down from one grid to the next one by one order

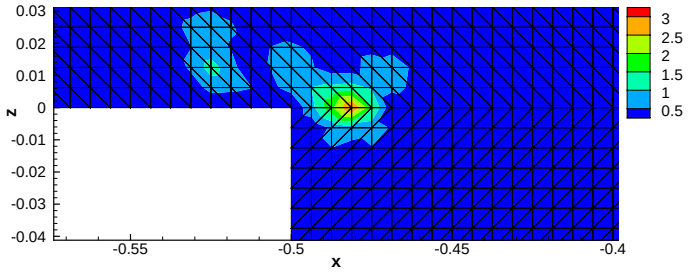

Fig. 10. Blow-up of the contour plot of the error of velocity u.

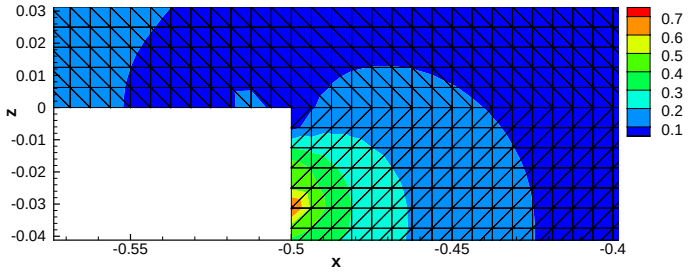

Fig. 11. Blow-up of the contour plot of the error of mass fraction Y_Q.

of magnitude. However, for the most interesting component of this calculation, the reaction product mass fraction Y_Q, we see in Table 6 a reduction of the maximum error by a factor 0.35 from grid 1 to 2 and by 0.48 from grid 2 to 3. For the mean errors hold factors 0.35 and 0.57, respectively.

Why is this error reduction so far away from the theoretically expected value? The reason is the above mentioned singularity of the Navier-Stokes equations at salient corners. The finer the grid, the better the singularity is detected, but the theoretically expected reduction of the error does not occur because the polynomial approach of the FDM cannot resolve a singularity. We must live with this fact. People that use standard software packages are not aware of that.

In conclusion we can say that the numerical solution of PDEs that includes an error estimate gives a quite new insight in the numerical result. Because of the singularity of the Navier-Stokes equations a total mesh refinement reduces the error only linearly, roughly by a factor of 0.5 instead of the expected reduction by an order of magnitude. How the singularity of the pure flow equations then affects the accuracy of the chemical components, e.g. of Y_Q, can only be seen from the error estimate of the numerical result.

References

1. Falconi, C.J., Denev, J.A., Fröhlich, J., Bockhorn, H., A test case for microreactor flows - a two-dimensional jet in crossflow with chemical reaction, Internal Report, available at `http://www.ict.uni-karlsruhe.de/index.pl/themen/dns/index.html`: "2d test case for microreactor flows. Internal report. 2007". This paper is included above in this file.

2. Schönauer, W., Adolph, T., FDEM: The Evolution and Application of the Finite Difference Element Method (FDEM) Program Package for the Solution of Partial Differential Equations, Abschlussbericht des Verbundprojekts FDEM, Universität Karlsruhe, 2005, available at `http://www.rz.uni-karlsruhe.de/rz/docs/FDEM/Literatur/fdem.pdf`
3. Schönauer, W., Scientific Supercomputing, Selfedition Willi Schönauer, 2000, E-Mail: `schoenauer@rz.uni-karlsruhe.de`